

**BROAD-SPECTRUM OPTICAL MULTIPURPOSE BLOOD-MONITOR  
(SwatBOMB)**

By  
Michael Yu-Herng Tu

Engineering 90: Senior Design  
Advisors: Erik A. Cheever, Ph.D and Lynne A. Molter, Sc.D  
Final Project Report

Submitted in partial fulfillment  
of the requirements for the degree of  
Bachelor of Science (B.S.)

Swarthmore College – Department of Engineering  
Swarthmore, PA  
5 May 2005

## Table of contents

List of Figures .....	3
List of Tables.....	3
List of Graphs.....	3
List of Appendices.....	3
ABSTRACT: .....	4
Abbreviations .....	5
Terms.....	5
1. INTRODUCTION .....	7
1.1 <i>Non-invasive optical blood monitoring</i> .....	7
1.2 <i>Broad-spectrum oximetry research</i> .....	8
2. BACKGROUND.....	8
2.1 <i>Two-wavelength transmission pulse oximetry: principles</i> .....	8
2.1.1 <i>The structure and function of hemoglobin</i> .....	9
2.1.2 <i>Absorption characteristics of hemoglobin and hemoglobin derivatives</i> .....	9
2.1.3 <i>Lambert-Beer's Law and oxygen saturation in hemoglobin</i> .....	10
2.1.4 <i>Arterial pulse characteristics</i> .....	12
2.1.5 <i>Calibration of the SaO<sub>2</sub> vs. R/IR curve</i> .....	13
2.2 <i>Known limitations of pulse oximetry</i> .....	13
2.3 <i>Extension to simultaneous evaluation of dysfunctional hemoglobins</i> .....	14
3. DESIGN CONSIDERATIONS .....	16
3.1 <i>Spectrophotometer configuration</i> .....	16
3.2 <i>Broad-spectrum light source</i> .....	16
3.3 <i>Finger cuff</i> .....	17
3.4 <i>Signal processing software</i> .....	17
4. ASSEMBLY AND IMPLEMENTATION.....	18
4.1 <i>Data acquisition</i> .....	18
4.2 <i>Signal Processing</i> .....	19
4.3 <i>Beer-Lambert Solution</i> .....	20
4.4 <i>Final system schematic</i> .....	21
5. RESULTS AND DISCUSSION.....	22
6. CONCLUSION.....	23
6.1 <i>Project limitations</i> .....	23
6.2 <i>Future work</i> .....	24
6.3 <i>General design evaluation</i> .....	26
References.....	27
APPENDICES .....	28

### List of Figures

FIGURE 1: OHMEDA 3700 PULSE OXIMETER.....	7
FIGURE 2: TRANSMISSION OXIMETRY GENERAL SCHEMATIC .....	8
FIGURE 3: STRUCTURE OF HEMOGLOBIN [6] .....	9
FIGURE 4: EXTINCTION COEFFICIENTS (E) RHB AND HBO <sub>2</sub> .....	10
FIGURE 5: BEER-LAMBERT LAW [8].....	10
FIGURE 6: LIGHT TRANSMISSION IN A VASCULAR BED. ....	12
FIGURE 7: BEER-LAMBERT MODEL AND EMPIRICAL CALIBRATION DISCREPANCIES.....	13
FIGURE 8: TYPICAL ADULT HEMOGLOBIN-OXYGEN DISSOCIATION CURVE .....	14
FIGURE 9: ABSORBANCE SPECTRA FOR HB, HBO <sub>2</sub> , COHB, AND METHB.....	15
FIGURE 10: SPECTRAL OUTPUT AND SPECTROMETER RESPONSE TO OCEAN OPTICS LS-1 .....	16
FIGURE 11: SWATBOMB BLOCK DIAGRAM SYSTEM SCHEMATIC .....	21
FIGURE 12: SWATBOMB IMPLEMENTATION .....	21

### List of Tables

TABLE 1: RESULTS USING 2-WAVELENGTH SOLUTIONS.....	22
--	----

### List of Graphs

GRAPH 1: CALIBRATION CURVE (ADJUSTED).....	20
GRAPH 2: MEAN VALUES FOR SAO <sub>2</sub> USING 2-WAVELENGTH MATRIX SOLUTION .....	22
GRAPH 3: MEAN VALUES FOR SAO <sub>2</sub> USING CALIBRATION CURVE.....	22

### List of Appendices

APPENDIX A: MATERIALS AND COSTS .....	28
APPENDIX B: SPECTROPHOTOMETER CONFIGURATION .....	29
APPENDIX C: SPECTRAL OUTPUTS FOR ALTERNATE LIGHT SOURCES .....	29
APPENDIX D: EXTINCTION COEFFICIENTS .....	29
APPENDIX E: FULL DERIVATION OF 4-COMPONENT SOLUTION .....	30
APPENDIX F: SAO <sub>2</sub> READINGS BY SUBJECT .....	32
APPENDIX G: FULL TABLE OF COMBINED RESULTS .....	34

**ABSTRACT:**

Noninvasive methods for blood monitoring have gained popularity in medical instrumentation. Commercial units generally quantify concentrations of specific blood constituents only. This goal of this project was to integrate and expand existing noninvasive blood-monitoring techniques into a robust broad-spectrum optical multipurpose blood-monitor (BOMB). The primary aim of the project was to expand standard oximetry techniques used in monitoring blood oxygen levels to a multi-wavelength system capable of simultaneously measuring *in vivo* oxygen, carbon monoxide, and methemoglobin concentrations. The project also sought to evaluate hardware and signal processing techniques used and to examine their viability in rigorous validation testing. The project will build on previous work in the department done by Corinne Bright '98, Mark Tong '99, and Jonathan Lee '03 [1],[2],[3]. Techniques employing a white light source and spectrophotometer provide a promising baseline for the implementation of additional optical techniques to a system capable of simultaneously monitoring hemoglobins, bilirubin and glucose.

**Keywords:** oximetry, broad-spectrum spectroscopy, multipurpose, optical, non-invasive, carboxyhemoglobin, methemoglobin, hemoglobins, dyshemoglobins

## Abbreviations

---

**COHb** – carboxyhemoglobin

**HbO<sub>2</sub>** – oxygenated hemoglobin; oxyhemoglobin

**LED** – light-emitting diode

**MetHb** – methemoglobin

**PPG** – photoplethysmogram

**RHb** – deoxyhemoglobin; reduced hemoglobin

**RMS** – root mean square

**R/IR** – red-to-infrared signal ratio

**SaO<sub>2</sub>** – oxygen saturation

**SwatBOMB** – Swarthmore Broad-spectrum Optical Multipurpose Blood-monitor

**VIS-NIR** – Visible-near infrared light

## Terms

---

**bilirubin** – reddish yellow water insoluble pigment occurring in bile and blood and causing jaundice if accumulated in excess

**carboxyhemoglobin (COHb)** – formed when CO bonds to hemoglobin. Elevated COHb saturation results in carbon monoxide poisoning.

**deoxyhemoglobin (RHb)** – see *reduced hemoglobin*

**dyshemoglobins** – hemoglobins where molecules other than oxygen have bonded to the heme carrying groups; dysfunctional hemoglobins

**in vivo** – within the human body

**in vitro** – outside the human body, in an artificial environment

**glucose** – optically active sugar. Glucose blood levels must be monitored carefully for patients with diabetes.

**hemoglobin** – iron-containing respiratory pigment in red blood cells consisting of a globin composed of four subunits, each linked to a heme submolecule, that functions in oxygen and carbon dioxide transport after conversions between deoxyhemoglobin and oxyhemoglobin in the lungs

**hypoxia** – condition of inadequate oxygen supply to tissues to maintain metabolic activity

**methemoglobin (MetHb)** – hemoglobin where change in coordination number of iron molecule in porphyrin ring renders it useless in gaseous transport

**oximetry** – determination of blood/tissue oxygen content, generally through optical means

**oxyhemoglobin (HbO<sub>2</sub>)** – hemoglobin with bound oxygen; oxygenated hemoglobin

**oxygenated hemoglobin (HbO<sub>2</sub>)** – see *oxyhemoglobin*

**pulse oximetry** – determination of oxygen saturation of pulsatile arterial blood by radiometric measurement of tissue optical absorbance curves

**reduced hemoglobin (RHb)** – hemoglobin with no bound oxygen; deoxyhemoglobin

## Acknowledgements

I have incurred many debts over the course of this year-long project, most substantively to Dr. Erik A. Cheever and Dr. Lynne A. Molter for their guidance, expertise, and patience. On countless occasions when I became lost and overwhelmed, their support placed me back on the right track. Edmond Jaoudi provided invaluable technical laboratory support both by locating miscellaneous items and also by promptly ordering those that were not immediately available. Crucial help in spectrometer configuration was provided by Denny Iwago and Harry Forsyth. Substantial gratitude is owed to Emily Blem at the University of Wisconsin – Madison for her heroic efforts in tracking down the M.S. thesis on which the 4-dimensional matrix solution is based. Similar thanks must be paid to the staffs of McCabe Library, Cornell Library, and Inter-Library Loan at Swarthmore College for handling and fulfilling the many requests I submitted over the course of the project. Thanks is due to past pulse oximetry students, most notably Mark Tong '99 for his initiation of the broad-spectrum multipurpose project, but also to Catherine Choi '96 and Corrine Bright '98 for their work on reflectance techniques and Jonathan Lee '03 for recent work on LED implementation; it is upon the foundation that they laid that this project was built.

## 1. INTRODUCTION

### 1.1 Non-invasive optical blood monitoring

Traditional methods for blood monitoring and determining the concentrations of various critical blood components require the invasive procurement of blood samples using a needle or skin-prick for *in vitro* analysis. Beyond inherent patient discomfort, the inconvenience and processing time requirements of such procedures constitute the primary drawbacks of existing technology. This in turn inhibits continuous real-time monitoring and results in barriers to enhanced monitoring and control of critical blood constituents. Dependence on invasive techniques, with its many drawbacks, therefore inhibits the efficient and tight control of this and other blood constituents.

New non-invasive methods not only amend such limitations, but also open new possibilities for patient care. Now-standard pulse oximetry methods have gained prominence for their ease of application for patient monitoring during anesthesia. Bilirubinometry has proven to be a valuable tool in diagnosing infantile jaundice. Forecasters have long envisioned noninvasive glucose monitoring and the possible development of a closed-loop system for automated insulin delivery for diabetes patients using closed-loop control. Non-invasive optical methods are thus an effective and attractive method with applications in anesthesiology, dermatology, and hematology.

The general approach behind optical non-invasive methods is to pass light through a vascular region of the body. The optical characteristics of skin and blood constituents are examined for unique transmission and reflection characteristics at certain wavelengths. Using signal processing and mathematical methods, the concentrations of various blood constituents concentrations can then be extracted from the spectral information of the transmitted beam. Given the completely noninvasive nature of such techniques, and the aforementioned drawbacks of invasive methods, the noted potential of optical methods for accurate and continuous determination of micronutrient concentration in real-time continues to invite considerable interest.

The successful development of non-invasive micronutrient monitors would represent a major advancement in the treatment and management of such conditions. Advancements in the availability of optical devices and signal processing software, and sustained research into the optical properties of skin and blood invite continued development of non-invasive optical methods.



FIGURE 1: OHMEDA 3700 PULSE OXIMETER

## 1.2 Broad-spectrum oximetry research

Standard oximetry instruments offer limited functionality but come at a high price. Most commercially available oximetry systems measure the transmission of narrow-band LED and laser diode emissions at two specific wavelengths (typically 660 nm and 940 nm). The specialization of these systems consequently limits their application to oxygen saturation and also depends on the assumption that deoxyhemoglobin and oxyhemoglobin are the only hemoglobin species present and ignores the incidence of dysfunctional hemoglobins, such as carboxyhemoglobin, methemoglobin, sulfhemoglobin, and hemoglobincyanide. The current oximetry techniques in standard use thus provide a limited view of blood composition, but also suffer from error under atypically high dysfunctional hemoglobin concentration.

While two-frequency analysis is sufficient for determining the concentration of two species, utilization of a broad-spectrum VIS-NIR light source and spectroscopy-based analysis would provide simultaneous transmission of a wider set of frequencies, and thus the simultaneous analysis a larger set of blood constituents for more complete and accurate blood monitoring. Research geared towards the detection of carboxyhemoglobin, bilirubin and glucose for carbon monoxide poisoning, infant jaundice and diabetes mellitus applications, respectively, receives the most attention from the private sector due to the considerable social demand for such tools [4].

## 2. BACKGROUND

### 2.1 Two-wavelength transmission pulse oximetry: principles

The appeal and widespread implementation of pulse oximetry lies in its completely noninvasive nature, its continuous and real-time application, and its ease of use. Assessment of expansion to broad-spectrum, spectroscopy-based applications should begin with a discussion of existing oximetry techniques, which serve as the baseline for design and whose inherent limitations must be considered.

The foundation of pulse oximetry relies on two primary principles: 1) that light absorbance of oxygenated hemoglobin ( $\text{HbO}_2$ ) differs from that of reduced (oxygen-deprived) hemoglobin (RHb) at red and infrared wavelengths, and 2) that absorbance at both wavelengths includes an AC component reflecting fluctuations in arterial blood volume between the light source and the transmission detector. The first provides the baseline considerations for oxygen concentration determination, while the second provides a means for isolating the optical activity of vascular blood from other human tissues. [5]. Such analysis draws upon knowledge of the structure of hemoglobin and hemoglobin derivatives and the biochemical foundations for spectroscopy-based analysis.

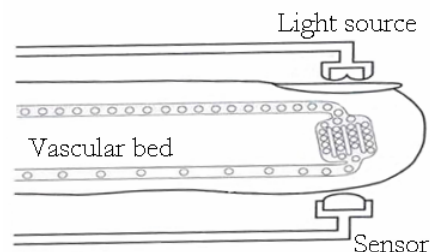


FIGURE 2: TRANSMISSION OXIMETRY GENERAL SCHEMATIC

### 2.1.1 The structure and function of hemoglobin

Hemoglobin is a porphyrin ring composed of two alpha and two beta chains. Hemoglobin molecules contain four subunit proteins, each containing a heme unit that typically binds to oxygen ( $O_2$ ) molecules. Reduced hemoglobin (figure 3b) occurs when nothing is bound to the heme units; it becomes oxyhemoglobin ( $HbO_2$ ) when bound to  $O_2$  (figure 3c).

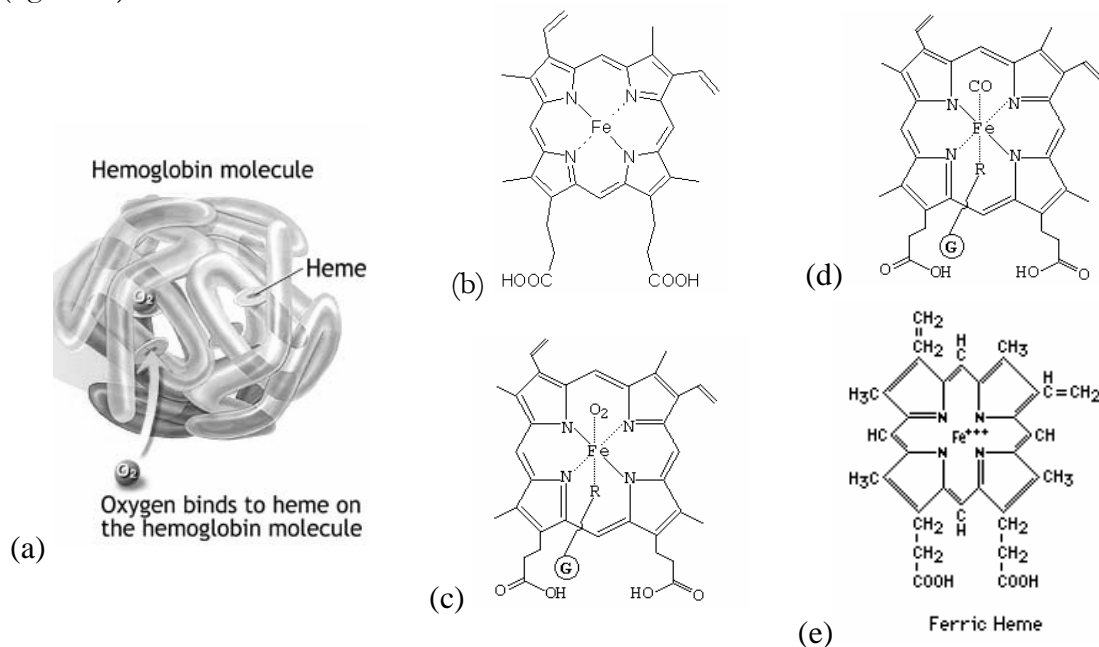


FIGURE 3: STRUCTURE OF HEMOGLOBIN [6]

(a) Each hemoglobin molecule contains 4 subunit heme, which binds to oxygen molecules in functional species. (b) Nothing is bound to the heme in RHB. (c) When oxygen binds to unbound heme in RHB, the result is  $HbO_2$ . RHB and  $HbO_2$  are known as the functional hemoglobins. (d) COHb occurs when carbon monoxide binds to the heme instead of gaseous oxygen. (e) Methemoglobin is produced by the occurrence of a ferric ion ( $Fe^{3+}$ ) rather than a ferrous ion ( $Fe^{2+}$ ) renders Hb unable to bind to  $O_2$  and thus is a cause of anemia. CoHb and MetHb are two examples of dyshemoglobins.

RHB and  $HbO_2$  are known as functional hemoglobins, as the structure of the molecule allows for its functionality in the transport of  $O_2$  throughout the body. However, the structure is occasionally disrupted and this function is inhibited. One such species is carboxyhemoglobin (COHb), which occurs when carbon monoxide binds to the heme groups (figure 3d). Overabundance of COHb is the cause of carbon monoxide poisoning. Another is methemoglobin (MetHb), which occurs when a ferric ion ( $Fe^{3+}$ ) rather than a ferrous ion ( $Fe^{2+}$ ) exists in the porphyrin ring (figure 3e). The changed coordination number also inhibits the transport of  $O_2$ , and abnormally high levels of MetHb result in methemoglobinemia, or a specific type of anemia. Each of these species of hemoglobin derivatives exhibits its own unique absorption spectra in the VIS-NIR region.

### 2.1.2 Absorption characteristics of hemoglobin and hemoglobin derivatives

The loading and unloading of oxygen or carbon monoxide, or the changes in the coordination number of the iron molecule, alters the electron distribution of the porphyrin ring. This redistribution results in different light absorption in the two states, which can be

noted visually through observable color differences between the oxygen-deprived deoxyhemoglobin (RHb) and oxygen-rich oxyhemoglobin (HbO<sub>2</sub>).

HbO<sub>2</sub> will absorb short wavelengths and appear bright red, whereas RHb will absorb longer wavelengths and appear a darker red [2]. This discrepancy in light absorption serves as the basis for the first principle behind optical detection of oxygen saturation through the transmission of two wavelengths: red ( $\lambda=600$  nm) and near-infrared ( $\lambda=940$  nm). The ratio between the concentrations of deoxygenated blood and oxygenated blood is proportional to the ratio of red light absorption to near-infrared light absorption, and Beer-Lambert Law can be used to extract absorbance information from transmission spectra. This proportionality is then used to compute arterial oxygen saturation.

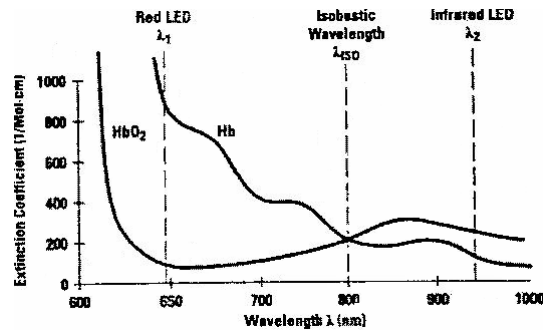


FIGURE 4: EXTINCTION COEFFICIENTS (E) RHB AND HBO<sub>2</sub>

Since  $E \propto A$ , the graph gives a proportionate representation of the absorption spectra for oxyhemoglobin and deoxyhemoglobin.[7]

### 2.1.3 Lambert-Beer's Law and oxygen saturation in hemoglobin

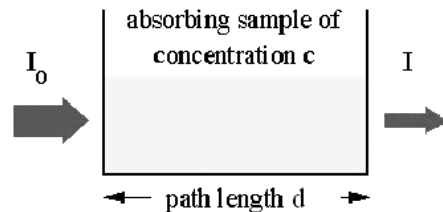


FIGURE 5: BEER-LAMBERT LAW [8]

Incident light intensity ( $I_0$ ) is related to transmitted light intensity ( $I$ ) by the extinction coefficient ( $\epsilon$ ), the concentration of the absorbing sample ( $c$ ), and the optical path length ( $d$ ). The extinction coefficient is a constant value for each species at each wavelength that becomes dimensionless when the ratio is taken. Optical path length is also eliminated in the matrix solution. This leaves an expression for the concentration of the sample in terms of the intensity of light transmission.

Light of intensity of  $I_0$  passing through an absorbing medium emerges with intensity  $I$ . Ignoring scattering and reflecting of light from surfaces, the Beer-Lambert Law states that the relationship between the two, at a given wavelength, will follow the relationship:

$$I = I_0 e^{-\epsilon cd}, \quad (\text{EQ. 1})$$

where  $\epsilon$  is the extinction coefficient,  $d$  is the distance traveled by the light (cm), and  $c$  is the concentration of the absorbing medium (mol/L). The expression can be re-written in the form

$$\epsilon cd = \ln\left(\frac{I_0}{I}\right) = -\ln\left(\frac{I}{I_0}\right) = A \quad (\text{EQ. 2})$$

where  $A$  is the absorbance, a dimensionless quantity defined as the natural logarithm of the ratio with the transmitted intensity over the incident intensity. A spectrophotometer can be used to obtain spectra as plots of absorbance versus wavelength. For a specific molecule or ion, this plot gives the characteristic spectrum of that particular molecule or ion [9]. For a mixture, however, the Beer-Lambert Law then states that the total absorbance of a mixture of elements with varying absorbencies is the sum of the individual absorbencies. Therefore, total absorbance at wavelength  $\lambda$  can be expressed as

$$A_\lambda = \epsilon_{\lambda 1} c_{\lambda 1} d_{\lambda 1} + \epsilon_{\lambda 2} c_{\lambda 2} d_{\lambda 2} + \dots + \epsilon_{\lambda n} c_{\lambda n} d_{\lambda n}, \quad (\text{EQ. 3})$$

where each  $\epsilon cd$  term corresponds to the absorbance contribution of each element. For the specific case of pulse oximetry, there are three relevant elements: 1) oxyhemoglobin, 2) deoxyhemoglobin, and 3) all other elements at two wavelengths: 1) red, and 2) infrared. Equation 3 can be written for this specific application as:

$$A_\lambda = \epsilon_{\lambda_{RHb}} c_{RHb} d + \epsilon_{\lambda_{HbO_2}} c_{HbO_2} d + \epsilon_{\lambda_x} c_x d + A_{\lambda_c}, \quad (\text{EQ. 4})$$

with  $d$  representing the contribution from deoxyhemoglobin,  $o$  representing the oxyhemoglobin contribution,  $x$  representing the contribution from all other elements, and the  $c$  term as the emitter/detector constant. As the last two terms can be assumed to remain constant, time derivatives written as the ratio between the rates of change for absorbencies of red and infrared light reduce as follows:

$$\frac{R}{IR} = \frac{dA_{\lambda(R)}}{dA_{\lambda(IR)}} = \frac{-d \ln\left(\frac{I_R}{I_0}\right) / dt}{-d \ln\left(\frac{I_{IR}}{I_0}\right) / dt} = \frac{\Delta I_R / I_{IR}}{\Delta I_{IR} / I_{IR}} = \frac{\epsilon_{R_{HbO_2}} c_{HbO_2} + \epsilon_{R_{RHb}} c_{RHb}}{\epsilon_{IR_{HbO_2}} c_{HbO_2} + \epsilon_{IR_{RHb}} c_{RHb}} \quad (\text{EQ. 5})$$

The saturation of oxygen can then be determined using this ratio and a calibration curve. Oxygen saturation ( $SaO_2$ ) is defined as the percentage of oxyhemoglobin to the sum of oxyhemoglobin and deoxyhemoglobin (note that any hypothetical presence of dyshemoglobins such as carboxyhemoglobin, methemoglobin and sulfhemoglobin are neglected in this expression). This can be written in terms of the equations defined in the Beer-Lambert Law as

$$SaO_2 = \frac{c_o}{c_o + c_d}, \quad (\text{EQ. 6})$$

which in turn can be written in terms of the R/IR ratio as

$$SaO_2 = \frac{\epsilon_{R_{RHb}} - \epsilon_{IR_{RHb}} \left(\frac{R}{IR}\right)}{\left(\epsilon_{R_{RHb}} - \epsilon_{R_{HbO_2}}\right) - \left(\epsilon_{IR_{RHb}} - \epsilon_{IR_{HbO_2}}\right) \left(\frac{R}{IR}\right)} \quad (\text{EQ. 7})$$

This expression serves as the basis for deriving oxygen saturation from the ratio of red to infrared transmission intensities.

#### 2.1.4 Arterial pulse characteristics

Determination of the ratio (R/IR) is based on the AC and DC components of the pulse form and can be best understood through the characteristic behavior of an arterial pulse. While hemoglobin is the strongest absorbing molecule in the blood, most of the total attenuation is due to light scattering and the opacity of the human finger. Pulse oximetry can be understood in light of the graphical display of red and infrared signals, or photoplethysmogram (PPG) to calculate oxygen saturation. The pulsatile arteries in the vascular bed, through constant contraction and expansion, modulate the light absorbance and produce a characteristic PPG waveform. While the amplitude and pulsatile component of the two waveforms differ, they share an almost identical shape which can therefore be used for the determination of oxygen saturation.

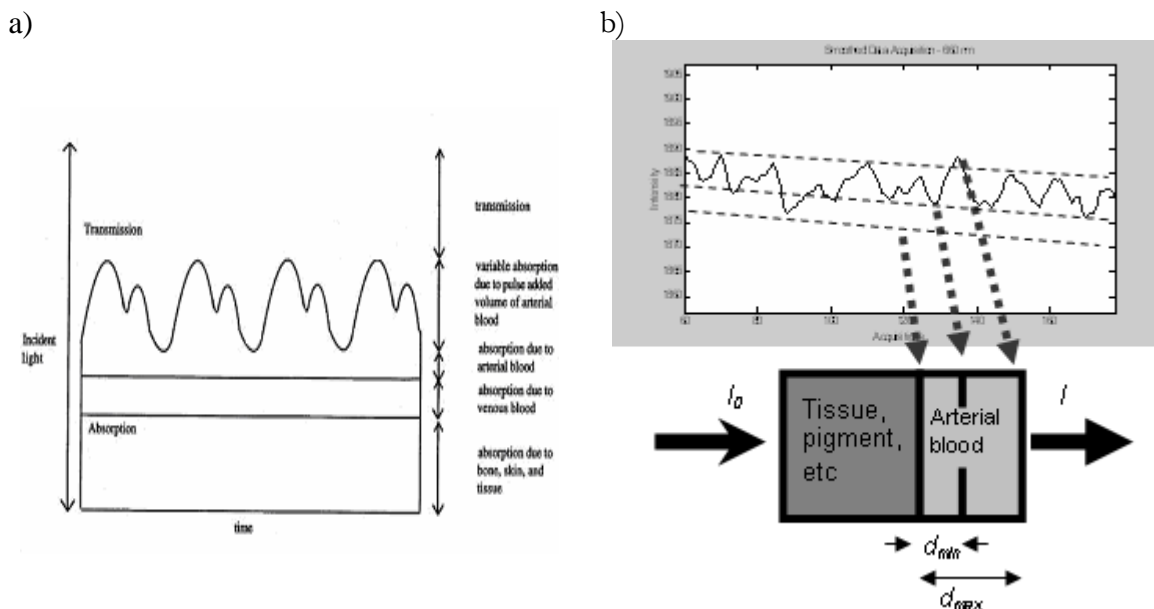


FIGURE 6: LIGHT TRANSMISSION IN A VASCULAR BED.

a) Normalizing light transmission by the variable component of the arterial blood can be used to isolate the absorption due to the arterial blood and its components. The AC component is the arterial pulse signal (roughly 1 Hz) and is used to determine  $SaO_2$ . [1]

b) A Beer-Lambert Law interpretation of the absorbance changes due to expansion and constriction of arteries during blood perfusion.

Constriction and expansion of the arterial diameter alters the optical pathlength during each pulse. Normalization of the intensity values by the variable component of the arterial blood isolates the absorption by arterial blood and its constituents. This

normalization of AC components by DC components is done by taking RMS value of the pulsatile component and dividing it by the mean of the original PPG:

$$\frac{R}{IR} = \frac{I_{R_{RMS}} / I_{R_{mean}}}{I_{IR_{RMS}} / I_{IR_{mean}}} \quad (\text{EQ. 8})$$

By a strict Lambert-Beer's Law solution, this value can then be substituted into equation 8 to solve for  $\text{SaO}_2$ . An alternate method employs empirically defined calibration curves.

### 2.1.5 Calibration of the $\text{SaO}_2$ vs. R/IR curve

Errors in the solutions yielded from the Beer-Lambert model are primarily due to the effects of light scattering [7]. Empirically defined curves are therefore employed in translating the R/IR ratio values into  $\text{SaO}_2$  values.

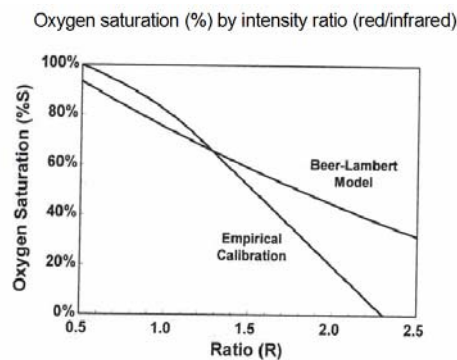


FIGURE 7: BEER-LAMBERT MODEL AND EMPIRICAL CALIBRATION DISCREPANCIES. Discrepancies due primarily to the effects of light scattering. [7]

Software tools developed by Corrine Bright '99 employed a linear calibration curve that is assumed to conform to the general function  $\text{SaO}_2 = (a-bR)/(c=dR)$ , where  $a-bR$  and  $c=dR$  are of the standard linear equation  $y=mx+b$  and  $m=R$ . The calibration curve used by Corinne Bright is shown below. The second driving principal behind pulse oximetry techniques incorporates methods that take advantage of nature of the signal from an arterial pulse. Pulse oximetry makes use of the fractional change in light transmission during an arterial pulse at the red and IR wavelengths. Spectrometer data across a finger will incorporate an AC component, attributed to variations in artery size during arterial wall contraction, and a DC component, which results from interaction with other material through which the light passes, such as skin and tissue. Also, the magnitude of these signals will vary from user to user.

## 2.2 Known limitations of pulse oximetry

While noninvasive optical analysis represents a noteworthy advance in patient monitoring, the inherent limitations of pulse oximetry should be reviewed before extending the application to simultaneous multi-constituent monitoring due to the reliance that may be placed on information derived from an oximetry-based system.

### 2.2.1. *Dyshemoglobin interference*

The primary functional weakness of the two-wavelength design lies in its limitation to the discrimination of only two species. High concentrations of other constituents with similar absorption properties presents a source for inaccuracy. Of particular concern are dyshemoglobins such as carboxyhemoglobin (COHb) and methemoglobin (MetHb), whose structural relation to RHb and HbO<sub>2</sub> result in similar light absorbance at oximetry wavelengths. Such interference causes readings to remain high even when the patient is hypoxic [10].

### 2.2.2. *Poor performance for low perfusion*

A normal pulse waveform is necessary for good pulse oximetry performance. However, situations such as hypothermia, hypotension, or the administration of vasoconstrictor drugs alter the arterial pulse characteristics and interfere with oximeter performance [11]. Patients with a history of vascular disease may also receive less accurate readings from pulse oximetry.

### 2.2.3. *Motion artifacts*

Disruption to the collection of PPG due to motion will result in inaccuracies in SaO<sub>2</sub> analysis. Care must therefore be taken to ensure that the probe is securely fastened to the skin and motion is minimized.

### 2.2.4. *Nonlinearity of the hemoglobin-oxygen dissociation curve*

The typical adult hemoglobin-oxygen dissociation curve is both nonlinear with decreasing slope and is virtually flat for high values of PaO<sub>2</sub> (see Figure 4). This characteristic shape suggests that attempts to relate SaO<sub>2</sub> with PaO<sub>2</sub> by linear regression, as is often the case in patient monitoring, meet serious difficulty in this range [5]. This implies that the pulse oximeter will generally fail to provide early warning of falling PaO<sub>2</sub> in contexts such as the operating room.

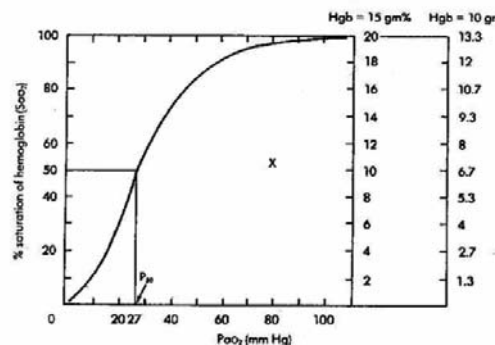


FIGURE 8: TYPICAL ADULT HEMOGLOBIN-OXYGEN DISSOCIATION CURVE  
(Arterial saturation plotted against oxygen partial pressure PO<sub>2</sub>)

## 2.3 Extension to simultaneous evaluation of dysfunctional hemoglobins

The next theoretical consideration is the feasibility of non-invasive optical monitoring methods in the determination of dysfunctional hemoglobins as an extension of the standard 2-wavelength pulse oximetry technique. Carboxyhemoglobin and

methemoglobin monitoring represents the most natural extension of pulse oximetry. The COHb and MetHb dyshemoglobin occurs when carbon monoxide instead of oxygen binds to the hemoglobin subunits, thus reducing the arterial oxygen transport and resulting in carbon monoxide poisoning. The similarities in molecular structure and absorption spectra are often cited as possible causes for error in pulse oximetry. However, these characteristics also purport that an extension of pulse oximetry to a three-wavelength module may feasibly be implemented in simultaneous determination of RHb, HbO<sub>2</sub>, COHb, and MetHb

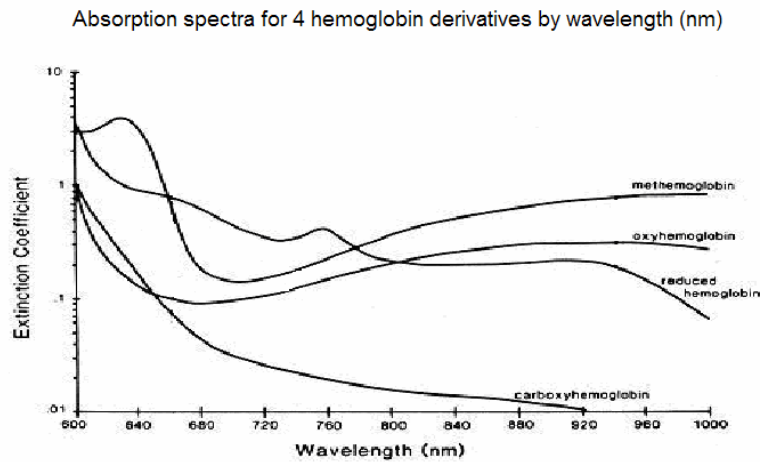


FIGURE 9: ABSORBANCE SPECTRA FOR HB, HBO<sub>2</sub>, COHB, AND METHB.

*The vertical dotted lines indicate the wavelengths used in pulse oximetry.[12]*

The basis for 4-component determination lies in a 4-dimensional solution to Beer's Law that makes mathematical use of absorbance ratios. The selection of wavelengths should depend on three factors: 1) in order to achieve a maximum difference in extinction coefficients; 2) relative flatness of the absorption spectra to minimize error due to wavelength imprecision; and 3) red skin pigments absorb at wavelengths less than 600 nm, so wavelengths should stay above that limit if possible.

A method for simultaneous evaluation of RHb, HbO<sub>2</sub>, and COHb saturations makes use of a pulse-oximeter system extended to three-wavelengths [13]. Absorption values are determined using a three-component version of equation 4. The three wavelengths are used for two absorbance ratios which, along with the assumption that the sum of the concentrations is 100%, gives a system of 3 linear equations in 3 unknowns that can be solved using a matrix solution. The coefficient for each of the unknown variables in the "absorbance ratio" equations can be expressed as:

$$A_{\lambda_1}\epsilon_{\lambda_2} - A_{\lambda_2}\epsilon_{\lambda_1} \quad (\text{EQ. 9})$$

The sum of these expressions is zero for each of the three "absorbance ratio" equations. The fourth equation used sums each of the concentrations to 100%. The complete derivation of this solution is given in Appendix E.

### 3. DESIGN CONSIDERATIONS

#### 3.1 Spectrophotometer configuration

Used for acquiring PPG data for multiple wavelengths, the availability of high-speed sampling over a broad wavelength band was the primary design requirement for the spectrophotometer. The Ocean Optics USB2000 Miniature Fiber Optic Spectrometer was selected on the basis of past success with the S2000 model, the availability of USB communication, sufficiently low integration and data transfer times, and upgraded data acquisition software with the USB2000.

Sufficient response to light transmission through a fairly opaque substance, such as a human finger, was critical. Related slit size, and optional accessories such as a collimating lens and a L2 detection collector lens. Additionally, anticipation of wavelengths of interest was necessary before selecting a grating. After consultation with Denny Iwago and Harry Forsyth at Ocean Optics, the configuration found in Appendix

#### 3.2 Broad-spectrum light source

The primary concerns are sufficient power for rapid spectrophotometer readings and that a relatively flat spectrum across the VIS-NIR section. The three options considered are discussed below:

##### 3.2.1. Tungsten Halogen Lamp (Ocean Optics LS-1)

The Ocean Optics LS-1 Tungsten Halogen Lamp was inherited from the ABMS implementation done by Mark Tong '99.[2] With successful implementation in the past, the LS-1 was designated as a baseline design choice. The LS-1 emits wavelengths in the VIS-NIR range (360-2000 nm). Replacement cost is \$499. Spectral output when measured with the USB2000 spectrometer appears below.

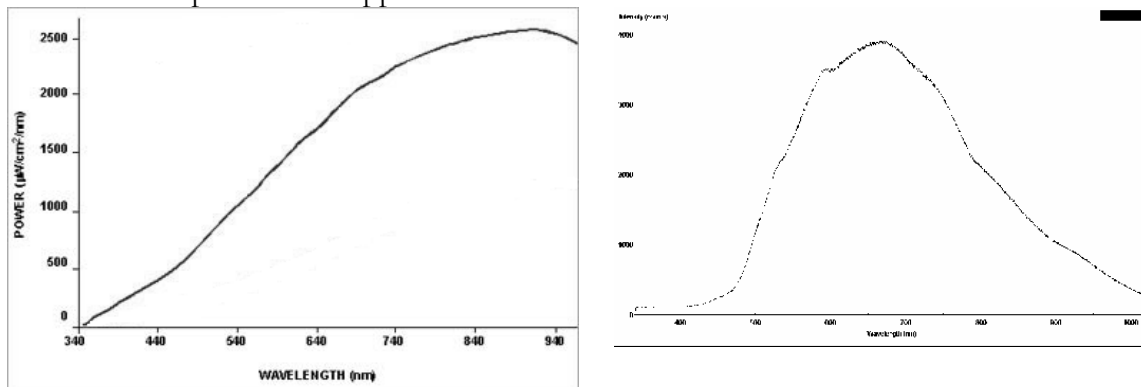


FIGURE 10: SPECTRAL OUTPUT AND SPECTROMETER RESPONSE TO OCEAN OPTICS LS-1

##### 3.2.2. Deuterium Tungsten Halogen Lamp (Ocean Optics MINI)

Deuterium Tungsten Halogen lamps combine the continuous spectra of Deuterium and Tungsten Halogen light sources. Such sources provide ample power across the VIS-NIR spectrum (roughly 500-1000 nm) and are available commercially from Ocean Optics. However, the performance enhancement over the in-house LS-1 model was determined to be insufficient, particularly with the considerable cost of the unit (~\$1400). The spectral output of the Ocean Optics MINI is available in Appendix C.

### 3.2.3. *Light-Emitting Diode (Lumileds High Power “Bright White” Luxeon Emmitter)*

The use of red and infrared LED sources in pulse oximetry applications has been previously explored by Jonathan Lee, '03 [3]. Several forms of white LED are commercially available. One form is made of a composite RGB chip and has a frequency distribution with three sharp peaks at 450 nm, 530 nm, and 640 nm. The serious fluctuation in power across the spectrum thus renders this type of LED of little interest.

A second variety, invented by the Nichia Corporation, uses a blue LED (typically InGaN) coated with YAG phosphors. The blue emission excites the phosphors which then produce a broad yellow light, and the two combine to form a white light. The most recent improvement, produced by Lumileds, double coats the blue LED, and is available in “high power” form. The spectral output for the Lumileds Luxeon “bright white” emitter can be found in Appendix

While the spectrum for the LED appears broad (see Appendix C), they are designed for power efficiency across the visible range (400 nm to 800 nm) and do not emit in the IR range. Potentially, a second LED could be used in conjunction to provide the full range. Bright white LED bulbs provide a considerable price advantage over the tungsten halogen lamp, but are more difficult to implement in comparison to the LS-1. Unfortunately, despite serious interest, time constraints inhibited the full exploration of a bright white + infrared LED lighting array.

### 3.3 **Finger cuff**

The finger cuff built by Mark Tong '99 was initially used for tested and three necessary improvements were identified. First, the relative spaciousness of the finger groove allowed for considerable motion artifact, and thus the size of the groove was reduced for a more rigid fitting cuff. Related to this is a second issue of ambient light. Whereas past implementations were not highly sensitive to ambient light, the new spectrometer employed produced a much more discernable pulse waveform when used in a closed environment with no light other than the LS-1 source. The black sheath surrounding the cuff was thus expanded to prevent ambient light transmission through the sides of the groove and finger entrance.

The Teflon construction was retained due to its advantages in minimizing temperature variation and a consequent constriction of blood arteries. However, the translucent white hue and reflective properties of the material presented a possible source of light scattering and diffraction within the cavity. The inside grooves were thus covered with a layer of black paper in an attempt to absorb the light and reduce interference due to the optical properties of the material.

### 3.4 **Signal processing software**

Initially, a general “rebuilding” of the ABMS system, evident in the design and implementation of hardware components, was foreseen for software tools. However, interest in utilizing the MatLab’s built-in filtering capabilities, as well as the relative ease of MatLab interfacing, required the full reconsideration of data processing tools and implementation in MatLab.

Band-pass filtering for the time acquisition PPG waveforms was performed using the internal functionality of MatLab. Specifically, the `firpm` function was used to generate a Parks-McClellan optimized equal ripple filter, and the PPGs were then filtered using the `filter` command. The `firpm` function accepts values for the cutoff frequency and transition

bands in terms of normalized frequencies and the point size of the filter. A 102-point filter was used with cutoff frequencies at 0.05 and 0.4 and a transition band of 0.01.

A peak-and-trough detector was attempted for the normalization of absorbance values. These values would have been substituted for RMS and mean values in equation 8 for a “ratio of ratios” algorithm [20]. A smoothing filter was used to extract the process the PPG so the indices of peaks and troughs, which could then be used to determine the exact magnitude from the original PPG. However, difficulties in assessing the validity of the ratios generated discouraged use of the MatLab functions created, and time constraints inhibited rigorous testing of the final results they generated. Thus, the RMS and mean values were used in normalizing the absorbance data as described in equation 8.

#### 4. ASSEMBLY AND IMPLEMENTATION

SwatBOMB implementation consists of three primary components: a) data acquisition; b) signal processing; and c) solving the Beer-Lambert solution, either by the matrix solution or the calibration curve. The issues and solutions encountered during the implementation of each stage are discussed in this section.



FIGURE 11: PRIMARY SYSTEM STAGES

##### 4.1 Data acquisition

The OOIBase32 software available for free with the USB2000 spectrometer successfully sampled transmission data at a rate of 19.6 Hz, thus successfully acquiring the PPG waveforms necessary. The modified finger cuff design (§3.3) sufficiently minimized motion artifact for a fairly stable PPG waveform.

The primary difficulty that was encountered was an unexpected characteristic response from the USB2000 spectrometer. Generally, time acquisitions would begin very high and then stabilize after roughly 600 acquisitions, or 40 seconds. This is believed to be due to the accumulation of charge in the CCD array in the spectrometer. Given the availability of a fairly regular and flat PPG at the end of the data acquisition, this “flat-portion” was simply extracted before the implementation of signal processing tools, and the first 600 acquisitions were disregarded.

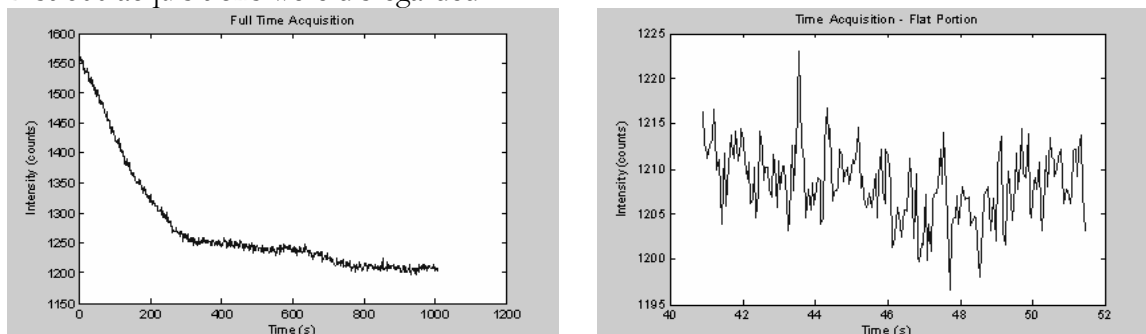


FIGURE 12: FULL AND “FLAT-PORION” TIME ACQUISITON (PPG SIGNALS)

#### 4.2 Signal Processing

The use of the MatLab `firpm` function for generating an optimized band-pass filter yielded a digital filter with the following magnitude response:

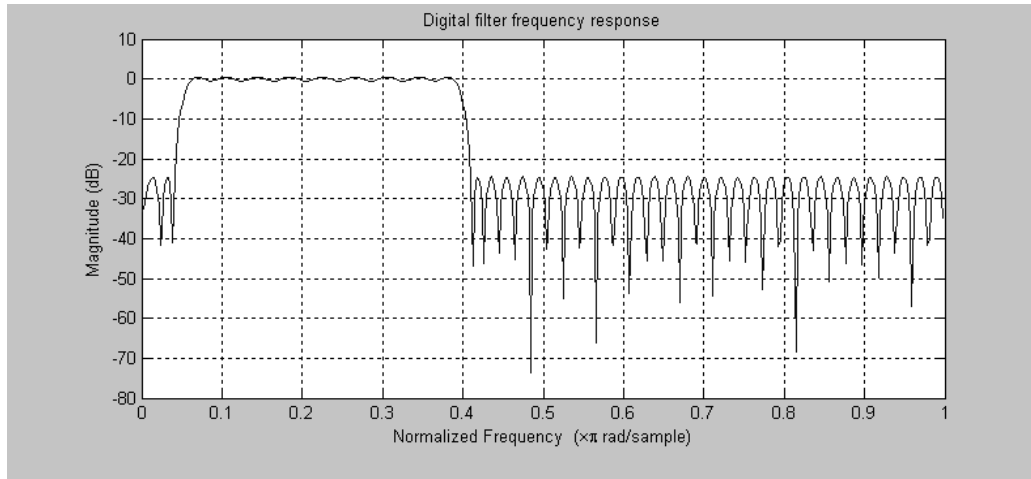


FIGURE 13: MAGNITUDE RESPONSE OF THE FIRPM-GENERATED DIGITAL FILTER

It was determined, however, that data filtered using this data had a non-zero DC component. Thus, a moving-average algorithm was implemented before the frequency band-pass filter in order to center the filtered PPG around zero to extract a meaningful RMS value for use in equation 8.

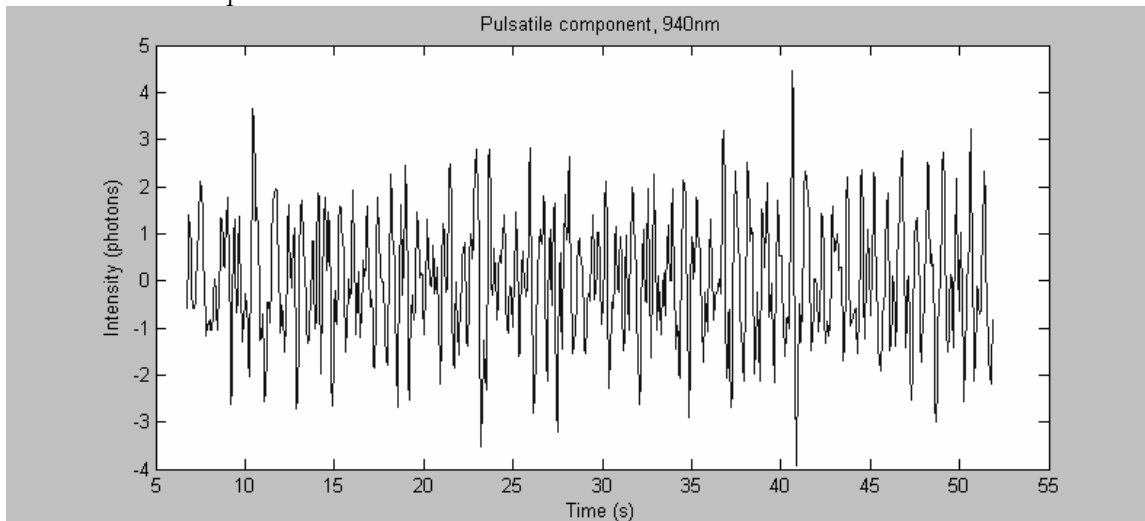
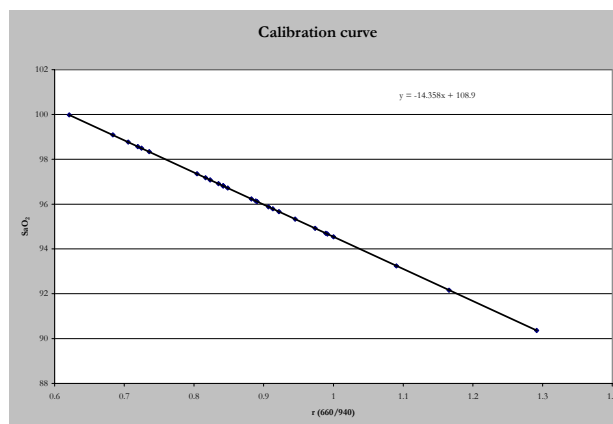


FIGURE 14: SAMPLE FILTERED PPG

### 4.3 Beer-Lambert Solution

Use of the 4-component solution (§2.3.1, Appendix E) yielded unreasonable results, with COHb concentrations typically around 80%, HbO<sub>2</sub> concentrations near 20%, and negative concentrations for RHb and MetHb. Adjustment of extinction coefficient values based on different published sources revealed that the system was highly sensitive to even small changes in extinction coefficient values. However, there were limited paths for assessing the sources of this error due to the unavailability of data for comparison. Thus, the matrix method was re-simplified to a 2-component system for comparison with the calibration curve method.

The calibration curve, based initially on that used by past oximetry students, initially gave an offset value. This offset was accounted for by adjusting the coefficients of the linear relationship.



GRAPH 1: CALIBRATION CURVE (ADJUSTED)

## 4.4 Final system schematic

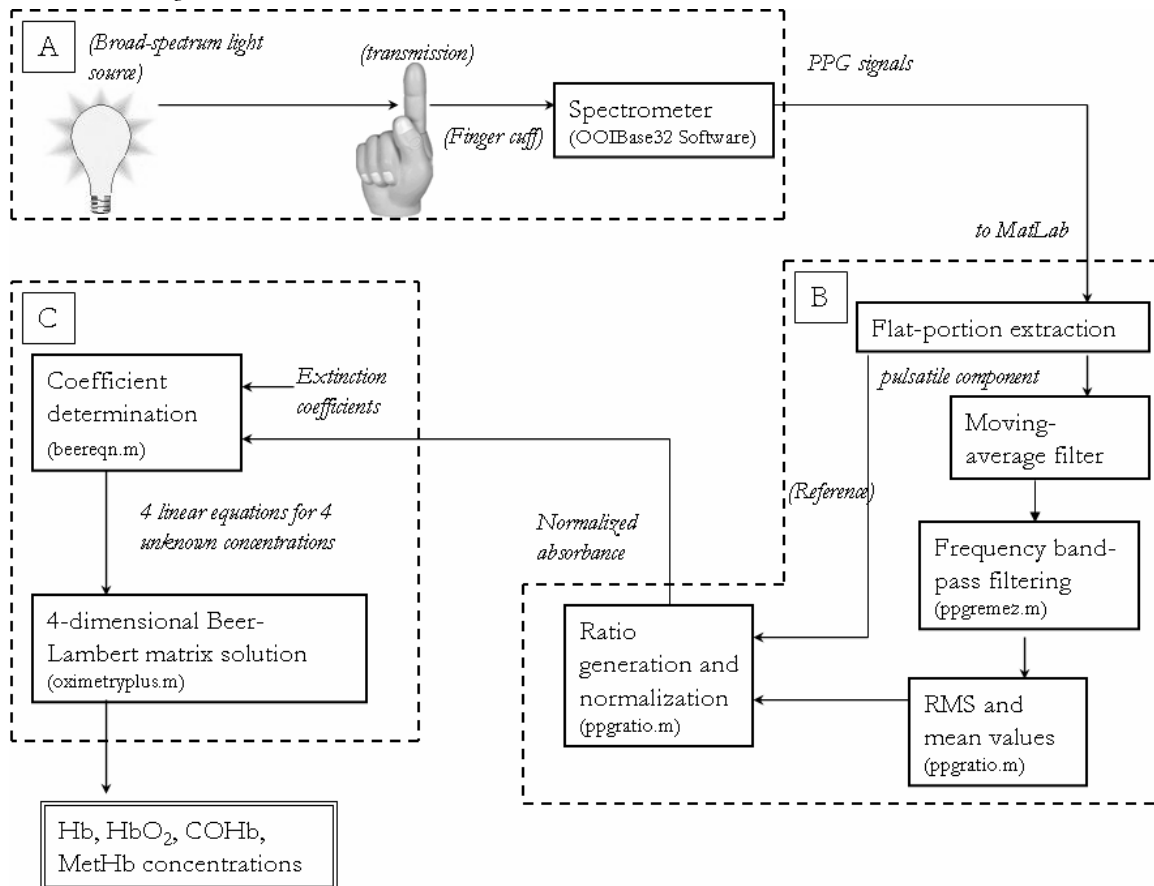


FIGURE 15: SWATBOMB BLOCK DIAGRAM SYSTEM SCHEMATIC

A – Data acquisition; B – Signal processing; C – Beer-Lambert Solution

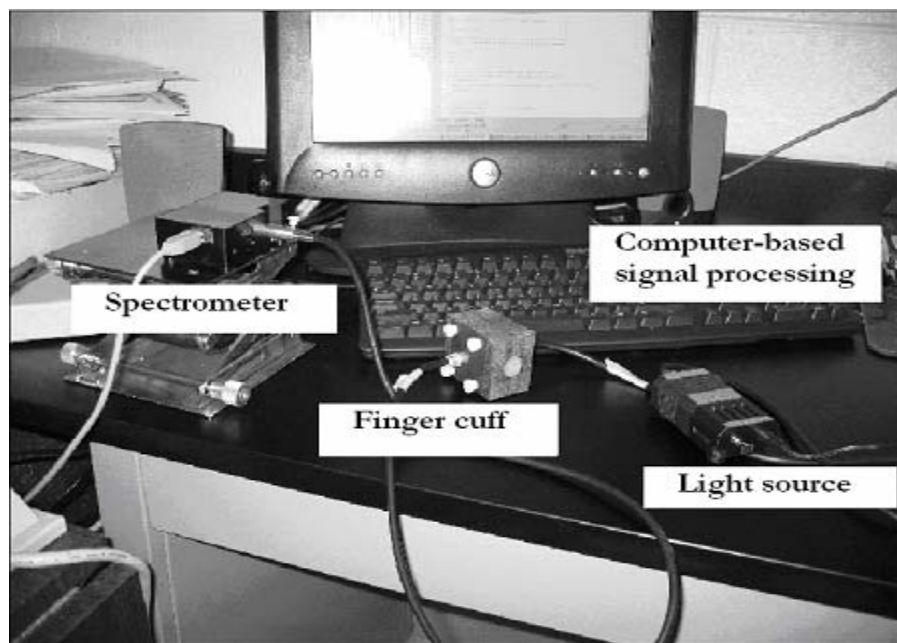
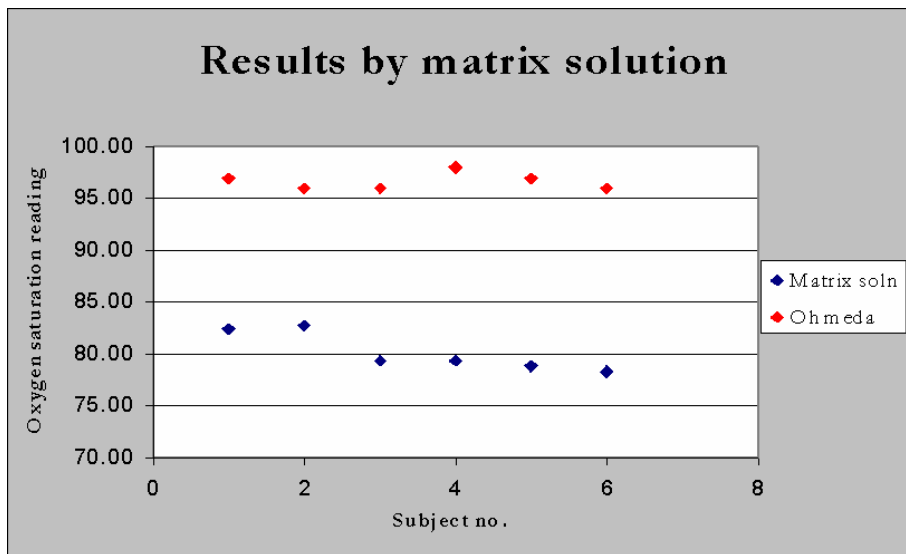


FIGURE 16: SWATBOMB IMPLEMENTATION

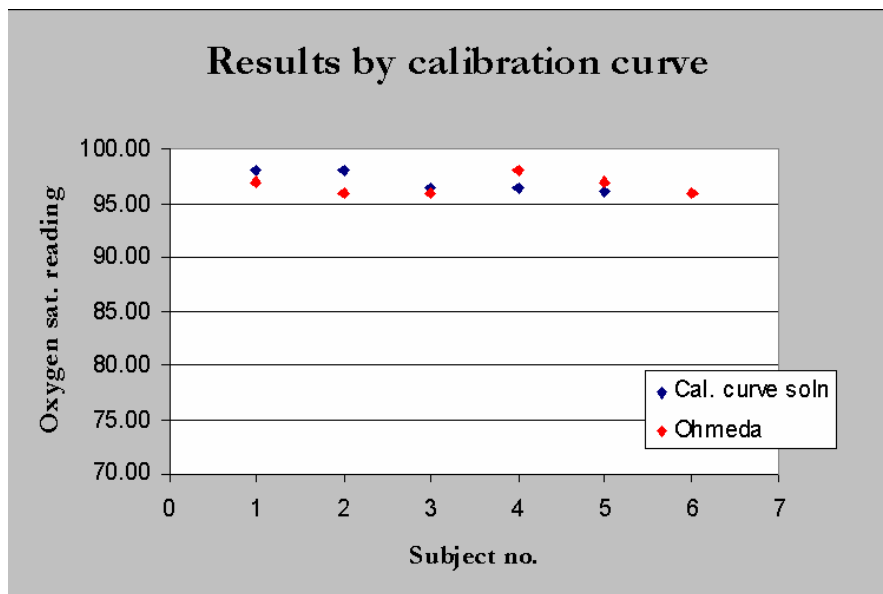
5. RESULTS AND DISCUSSION

Subject no.	n	669/940	SaO <sub>2</sub> (Matrix solution)	SaO <sub>2</sub> (Cal. Curve)	Ohmeda	% error (Ohmeda-Cal. curve)
1	5	0.96914 ± 0.19	76.09 ± 5.91	94.98509 ± 2.76	97	2.1
2	3	0.975667 ± 0.17	75.84 ± 5.22	94.89138 ± 2.41	97.5	2.7
3	5	0.86616 ± 0.09	79.29 ± 3.13	96.46367 ± 1.38	96.5	1
4	5	0.72104 ± 0.21	84.07 ± 6.48	98.54731 ± 3.01	96.5	2.1
5	5	0.94592 ± 0.04	76.71 ± 1.38	95.31848 ± 0.62	98	2.7
6	4	0.853275 ± 0.17	79.77 ± 5.49	96.64868 ± 2.46	97	1.6

TABLE 1: RESULTS USING 2-WAVELENGTH SOLUTIONS



GRAPH 2: MEAN VALUES FOR SAO2 USING 2-WAVELENGTH MATRIX SOLUTION



GRAPH 3: MEAN VALUES FOR SAO2 USING CALIBRATION CURVE

Table 1 gives a summary of mean values oxygen saturation determination results for each subject using the matrix solution, the calibration curve, and using the Ohmeda standard. The high discrepancy between the matrix solution and the calibration curve, somewhat expected based on the discrepancy shown in figure 7, can be seen in the different results from the two solutions.

This discrepancy can be seen graphically through a comparison of Graph 1 and Graph 2. Graph 1 gives a graphical representation of the results of the matrix solution, with oxygen saturation readings typically near 80% and with an average magnitude of error near 18%. However, the relatively stable discrepancy encourages the application of a calibration curve.

Graph 2 gives the results when the ratios are translated into saturation values using a calibration curve rather than the strict Beer-Lambert model equations. The general linear form was taken, and coefficients were adjusted based on expected results (no standard coefficients are provided in the literature, because the sources of error for each system are highly specific to the material and configuration used). These results generally conform to the Ohmeda system. Given in Table 2, the system gives absolute standard deviations generally under 3 for each subject, and percent errors also under 3%. However, the small number of subjects (6), the limited number of total trials (27) and lack of consideration of other variables, such as complexion and skin temperature, invite a more nuanced and comprehensive evaluation of the validity of the calibration curve used.

## 6 CONCLUSION

### 6.1 Project limitations

#### 6.1.1 *High cost*

The current implementation runs at a very high cost of roughly \$3000. Meanwhile, the system remains limited to a 2-wavelength solution. However, the primary consideration in selecting components was versatility and ease of expansion for multiple modules in the future. As the current implementation is designed primarily for concept validation and experimentation; a version designed to be competitive in price with other oximeters might consider different light sources or pulsed sensors for the particular wavelengths of interest.

#### 6.1.2 *Limited scope of calibration curve*

Only healthy adults were available for trials. Although the employed curve yields percent errors under 1%, readings are limited to the interval between 96% and 98% oxygen saturation. The validity of the model outside of this region and for unhealthy subjects, where accuracy is most crucial, is unknown. Also, little attention was paid to lurking variables such as complexion and body temperature. A more comprehensive evaluation of the calibration curve would include a more nuanced statistical analysis.

#### 6.1.3 *Time requirements for data acquisition*

Current treatment of the response of the spectrometer shown in figure 12 necessitates long data acquisitions. This is somewhat prohibitive to the application of such a system for effective patient monitoring.

## 6.2 Future work

The numerous limitations of the current SwatBOMB implementation invite future evaluation and experimentation. Most glaring is the lack of statistically significant results over the full spectrum of blood oxygen levels and the lack of an effective multipurpose module. However, the work described in this report represents a promising foundation upon which further work might be drawn. Possible avenues for attacking these limitations include:

### 6.2.1 *Rigorous calibration curve testing*

More nuanced and varied empirical testing would enhance the validity of the system for the reasons discussed in 6.2.1. Specific variables to consider include skin pigmentation (whereas the effects should theoretically be eliminated by isolation of the pulsatile component, the effect of complexion on the light scattering effects that cause the disparity between empirical and theoretical curves should be further explored), a potential wider scope beyond only healthy subjects, and replication for statistical significance.

### 6.2.2 *Empirical curves for the 4-component system*

The two-component solution tested is essentially a two-variable matrix solution but solved explicitly for  $\text{SaO}_2$ . If the use of empirical curves corrects the errors and offsets due to scattering effects in the two-variable solution, the viability of empirical calibration for the 4-wavelength solution should be explored.

### 6.2.3 *Nonlinear modeling for the 4-component system*

Results for the 4-component matrix solution yielded unreasonable results, often with negative values for concentrations. The solutions for mathematical model would be subject to nonlinear constraints, such as an asymptote at zero percent concentration.

### 6.2.4 *Phantom (artificial finger)*

The Ohmeda Biox 3700 currently serves as our standard for comparison. However, a new standard would be necessary for rigorous validation of a 4-component solution. *In vitro* analysis of live samples as a standard would require expertise in biochemical analysis techniques. A promising compromise is the construction of a phantom, or artificial finger, that models the optical characteristics of human skin and tissue and the arterial pulse characteristics. Analysis for controlled concentrations can then be performed.

### 6.2.5 *Non-hemoglobin blood constituents*

Difficulty was encountered in the expansion of the 2-component oximetry solution to a 4-component oximetry solution. However, this should not preclude investigation into the combination of 2-component oximetry and non-hemoglobin blood constituents.

#### 6.2.5.1 *Bilirubin*

Absorption spectroscopy methods for determining bilirubin levels have been developed for the treatment of bilirubinemia [14]. Hyperbilirubinemia, common in neonates, is the accumulation of bilirubin because the liver has not yet developed enzymes for oxidizing bilirubin. Increased levels of cutaneous bilirubin cause jaundice; extreme cases

will result in bilirubin precipitation into the brain, causing kernicterus, or permanent brain damage. Noninvasive bilirubin monitoring is a particularly attractive method for infant care.

Commercial optical bilirubin monitors are currently manufactured by SpectRx, Inc and Minolta [15]. The predominant method for measuring cutaneous bilirubin levels depends on measuring the reflectance of light off skin. The reflectance spectrum is then used to determine the absorption coefficient, which is proportional to bilirubin concentration [16]. Bilirubin determination was initially envisioned as a possible extension should the project ever progress to reflectance techniques. With the decision to concentrate on transmission-based determination, bilirubin determination was ultimately not pursued. However, given reflectance sensors, the system can be easily expanded to include a bilirubin determination module.

#### 6.2.5.2 *Glucose*

Great interest has been invested in the potential development of a non-invasive optical glucose monitoring system due to the tight control necessary for diabetes mellitus patients and the desirability of closed-loop insulin level control. However, the optical characteristics of glucose render glucose determination beyond the scope of materials easily available today. Attempts to monitor arterial glucose levels with methods that could be integrated into SwatBOMB would require light source and spectrometry capabilities at the low-infrared region from around 1650nm-3650nm. As commercially available optical components tend to focus on the visible and near-visible light range (450 nm – 900 nm), inclusion of a glucose module would require either considerable investment in procuring light generation and spectrometry capabilities at these wavelengths, or more fundamental research into developing techniques utilizing the wavelengths currently available.

The number of promising analytical tools being developed for the *in vivo* measurement of glucose by near-infrared (NIR) spectroscopy are considerable. These include partial least squares (PLS) regression, Fourier filtering, and Monte Carlo integration [17], [18]. Investigation of such techniques were beyond the scope of this investigation due to time and materials constraints. Other noninvasive methods for monitoring glucose saturation, essential in the treatment of diabetes, include absorption spectroscopy, polarimetry, raman spectroscopy, and fluorescence monitoring [4]. Attempts to monitor arterial glucose concentrations *in vivo* using absorption spectroscopy have met considerable difficulty, and the analytical feasibility of glucose determination remains ambiguous, which is unfortunate given the considerable market interest [19].

#### 6.2.6 *Reflection spectroscopy-based broad spectrum analysis*

The advantages of reflection-based oximetry include prenatal monitoring of fetal blood. Fetal blood analysis is further complicated by the discrepancy between absorbance characteristics in adult and fetal blood [17].

#### 6.2.7 *LED light source*

The advantages of the LED light source include cost benefits and lower power consumption. Recent advances in the quality of the spectrum of white LEDs and the availability of “bright white” LEDs from Nichia and Lumileds potentially allows for LED implementation using one bright white bulb and one infrared bulb.

### 6.3 General design evaluation

An analysis of inventory and impact addressed the following realistic design constraints and practical considerations:

#### 6.3.1. *Economic*

The considerable cost of the system is a result of the interest in robust design and ease of addition. Despite the considerable cost of system components, sustained attention towards the development of additional functionality, including further investigation into the 4-component matrix solution and the possibility of bilirubinometry and glucose monitoring, benefit from the robust design.

#### 6.3.2. *Manufacturability*

All materials will be either purchased off the shelf or made in the machine shop at Swarthmore. Thus, given the low fabrication requirements, SwatBOMB assembly was relatively straightforward and of minimal time and cost.

#### 6.3.3. *Environmental*

The current goals of concept proof do not involve fabrication, combustion or significant waste disposal and therefore pose no environmental threat. Furthermore, the system prototype presents no pollutant or radiation threat to its surroundings. SwatBOMB, within its current conceptual context as well as in future development, poses no significant environmental concerns.

#### 6.3.4. *Sustainability*

Given the relatively short time frame involved, there was no equipment retirement due to ageing for the duration of this project. A hypothetical life cycle analysis of the design, development, operation and disposal of SwatBOMB, with components selected, will forecast the use of materials over the course of the project. Initial costs include a PC workstation, a diffraction grating spectrometer, a broad-spectrum light source, fiber-optic cables, a Teflon cuff, and software development tools, and the life-cycle of these components and the cost of replacement dictates sustainability concerns of an eventual product. A final product would have a life-cycle determined by the life of the white light source and the fiber-optic light source.

#### 6.3.5. *Ethical*

There are no foreseeable unethical applications or ethical concerns. Widespread and uncontroversial use of commercial oximeters, and the similarity of SwatBOMB in function and application, supports this claim.

#### 6.3.6. *Health and safety*

The current context of SwatBOMB remains that of concept proof and validation. Following further development, any future commercial production for use in medical practice must follow extensive and rigorous validation testing beyond the scope of that which will be performed here. Also, the limitations of optical noninvasive monitoring (§2.2) must be considered when making medical decisions based on oximetry data.

### 6.3.7. Socio-political

The considerable costs of various system components (Appendix A) raises concern regarding per-unit cost and overall healthcare expenses. The multifunctional inclusion of several constituent saturation determination modules, however, and the social benefits of noninvasive blood analysis in patient comfort, safety, and prospects for development of closed-loop control offsets such concerns.

## References

1. Bright, C., *Noninvasive Optical Monitoring: Laser Diode-Based Reflectance Pulse Oximetry*. Senior Design Projects, Department of Engineering, Swarthmore College, 1998. **1**.
2. Tong, K.M.M., *Extending Pulse Oximetry: Design and Development of a broad-spectrum, spectroscopy based Arterial Blood Monitoring System*. Senior Design Projects, Department of Engineering, Swarthmore College, 1999. **5**.
3. Lee, J., *Light Emitting Diode (LED): Reflectance Pulse Oximetry*. Senior Design Projects, Department of Engineering, Swarthmore College, 2003. **3**.
4. Coté, G.L., *Noninvasive and minimally-invasive optical monitoring techniques*. Journal of Nutrition, 2001. **131**: p. 1596S-1604S.
5. Barker, S.J., K.K. Tremper, *Pulse Oximetry: Applications and Limitations*. International anesthesiology clinics, 1987. **25**(3): p. 155-175.
6. *Blood Disorders*. 2005, Shands Health Care.
7. Flewelling, R., *Noninvasive Optical Monitoring*, in *The Biomedical Engineering Handbook*. 1995, CRC Press: IEEE Press: Boca Raton. p. 1346-1352.
8. Tissue, B.M., *Beer-Lambert Law*, in *Hypermedia for Science Education*. 1996.
9. Meissler, G.L.a.D.A.T., *Inorganic Chemistry*. 3rd ed. 2004, Upper Saddle River, NJ: Pearson Prentice Hall. 380-381.
10. Kamat, V., *Pulse Oximetry*. Indian Journal of Anesthesiology, 202. **46**(4): p. 261-268.
11. Yelderman M, N.W.J., *Evaluation of pulse oximetry*. Anesthesiology, 1983. **59**: p. 349-352.
12. Eisenkraft, J., and SJ Barker, *Monitoring oxygen and ventilation*, in *Cardiac, vascular, and thoracic anesthesia*, J. Youngberg, Editor. 2000, Churchill Livingstone: New York, NY. p. 307-327.
13. Buinevicius, R., *A three-wavelength pulse oximeter for carboxyhemoglobin determination*, in *Department of Electrical and Computer Engineering*. 1987, University of Wisconsin - Madison: Madison. p. 34.
14. Saidi, I.S., Jacques S.L., Tittel F.K., *Monitoring neonatal bilirubinemia using an optical patch*. SPIE Proc, 1990. **1201**: p. 569-578.
15. Robertson, A., Steve Kazmierczak, and Paul Vos, *Improved Transcutaneous Bilirubinometry: Comparison of SpectRX BiliChecx and Minolta Jaundice Meter JM-102 for Estimating Total Serum Bilirubin in a Normal Newborn Population*. Journal of Perinatology, 2002. **22**: p. 12-14.
16. Jacques, S.L., Iyad Saidi. et al. *Developing an optical fiber reflectance spectrometer to monitor bilirubinemia in neonates*. in *Laser-Tissue Interactions*. 1997. San Jose, CA: SPIE Proceedings.
17. Marquardt, L.A., Mark A. Arnold, and Gary W. Small, *Near-Infrared Spectroscopic Measurement of Glucose in a Protein Matrix*. Analytical Chemistry, 1993. **65**: p. 3271-3278.

18. Small, G.W., Mark A. Arnold, and Lis A. Marquardt, *Strategies for Coupling Digital Filtering with Partial Least-Squares Regression: Application to the Determination of Glucose in Plasma by Fourier Transform Near-Infrared Spectroscopy*. Analytical Chemistry, 1993. **65**: p. 3279-3289.
19. Arnold, M.A., *Non-invasive glucose monitoring*. Current Opinion in Biotechnology, 1996. **7**: p. 46-49.
20. Webster, J.G., *Design of Pulse Oximeters*. 1997, Bristol: Institute of Physics Publishing.
21. Zijlstra, W., Buursma, A, and van Assendelft, OW, *Visible and near infrared absorption spectra of human and animal hemoglobin*. 2000, Utrecht: VSP.

## APPENDICES

### APPENDIX A: MATERIALS AND COSTS

#### Optoelectronics:

Item	Description	Cost	Notes
Ocean Optics USB2000	Commercial high-speed spectrometer	\$2499	\$500 trade-in offer. Configuration in Appendix B.
Ocean Optics LS-1	Tungsten-halogen lamp for bright white transmission	---	Available from Mark Tong's research; replacement cost of \$499
Fiber bundle		---	Available from Mark Tong's research
Lumileds Bright White Luxeon Emitter	High power, low cost visible-region (400-800 nm) light source. Relatively flat spectrum	\$5.98	Emitter model requires MCPCB; built into Star model (\$8.50)
MCPCB for Luxeon Emitter	Heat sink for Luxeon Emitter	*	Obtained as free sample
Nichia 5-mm Bright White LED	5-mm bright white LED light source. Similar spectrum with Luxeon	*	Obtained as free sample

#### Software

Item	Description	Cost	Notes
OOI Base32	Supplied software for USB2000	Free	
MatLab	Used for signal processing and Beer-Lambert solutions	Free*	Academic license used for educational purposes

#### Miscellaneous

	Description	Cost	Notes
Dell Optiplex	CPU for	Free*	Available in-house

**APPENDIX B: SPECTROPHOTOMETER CONFIGURATION**

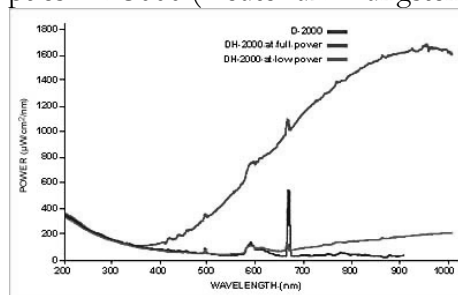
Spectrophotometer configuration and price quote

Item Code	Item Description	Price
USB2000	USB2000 Plug-and-Play Spectrometer, USB & serial interface	\$2199.00
GRATING #4	Grating 4, installed, 350-1000 nm	
OFLV-350-1000	Order-sorting detector filter, VIS, installed in "S" bench	\$150.00
SLIT-200	Installed optical bench entrance aperture, 200-micron width	\$150.00
Total:		\$2499.00

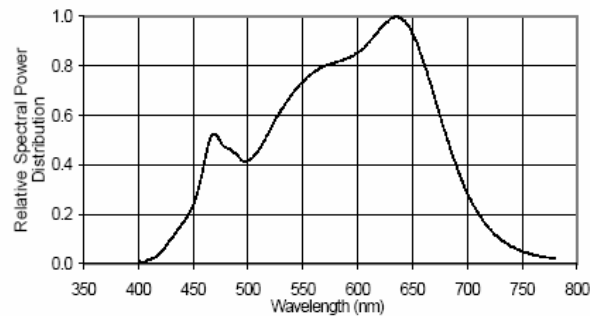
**APPENDIX C: SPECTRAL OUTPUTS FOR ALTERNATE LIGHT SOURCES**

Spectral output for alternate white light sources

Ocean Optics DH3000 (Deuterium-Tungsten-Halogen)



Lumileds Luxeon 'Bright White' Emitter

**APPENDIX D: EXTINCTION COEFFICIENTS**

Extinction coefficients

	Adult deoxyhemoglobin (haemoglobin)	Adult oxyhemoglobin (oxyhaemoglobin)	Adult carboxyhemoglobin (carboxyhaemoglobin)	Adult methemoglobin (haemoglobin)
660 nm	3.26	0.4	0.27	3.78
740 nm	0.7874	1.3502	0.07	2.8
840 nm	1.35	0.54	0.0840	0.98
940 nm	0.7815	1.1072	0.008	2.7

Values taken from Zijlstra, et al. [21]

## APPENDIX E: FULL DERIVATION OF 4-COMPONENT SOLUTION

Equation 3 gives an equation for the absorbance in terms of extinction coefficient ( $\epsilon$ ), optical pathlength ( $d$ ) and concentration ( $c$ ) for an  $n$  component mixture. This equation can be stated explicitly in terms of RHB, HbO<sub>2</sub>, COHb, and MetHb in terms of a specific frequency  $\lambda$  as follows:

$$A_{\lambda} = \epsilon_{\lambda_{RHB}} c_{RHB} d + \epsilon_{\lambda_{HbO_2}} c_{HbO_2} d + \epsilon_{\lambda_{COHb}} c_{COHb} d + \epsilon_{\lambda_{MetHb}} c_{MetHb} d$$

The four chosen wavelengths were 660 nm, 940 nm, 740 nm, and 840 nm. 660 nm and 940 nm were chosen due for ease of troubleshooting, as they are prevalent in 2-wavelength oximetry systems. 740 nm and 840 nm were chosen based on a qualitative assessment of the absorbance spectra and with the criteria outlined in §2.3. The four absorbance equations, stated explicitly, then are:

$$\begin{aligned} A_{660} &= \epsilon_{660_{RHB}} c_{RHB} d + \epsilon_{660_{HbO_2}} c_{HbO_2} d + \epsilon_{660_{COHb}} c_{COHb} d + \epsilon_{660_{MetHb}} c_{MetHb} d \\ A_{940} &= \epsilon_{940_{RHB}} c_{RHB} d + \epsilon_{940_{HbO_2}} c_{HbO_2} d + \epsilon_{940_{COHb}} c_{COHb} d + \epsilon_{940_{MetHb}} c_{MetHb} d \\ A_{740} &= \epsilon_{740_{RHB}} c_{RHB} d + \epsilon_{740_{HbO_2}} c_{HbO_2} d + \epsilon_{740_{COHb}} c_{COHb} d + \epsilon_{740_{MetHb}} c_{MetHb} d \\ A_{840} &= \epsilon_{840_{RHB}} c_{RHB} d + \epsilon_{840_{HbO_2}} c_{HbO_2} d + \epsilon_{840_{COHb}} c_{COHb} d + \epsilon_{840_{MetHb}} c_{MetHb} d \end{aligned}$$

Taking ratios allows of two absorbance values allows us to eliminated the variable  $d$  for optical path length. While  $d$  should remain relatively constant, its variability can nevertheless be eliminated altogether by taking absorbance ratios. The three ratios chosen were 940/660, 660/840, and 740/940. Taking these three ratios and eliminating the variable  $d$  give:

$$\begin{aligned} \frac{A_{940}}{A_{660}} &= \frac{\epsilon_{940_{RHB}} c_{RHB} + \epsilon_{940_{HbO_2}} c_{HbO_2} + \epsilon_{940_{COHb}} c_{COHb} + \epsilon_{940_{MetHb}} c_{MetHb}}{\epsilon_{660_{RHB}} c_{RHB} + \epsilon_{660_{HbO_2}} c_{HbO_2} + \epsilon_{660_{COHb}} c_{COHb} + \epsilon_{660_{MetHb}} c_{MetHb}} \\ \frac{A_{660}}{A_{840}} &= \frac{\epsilon_{660_{RHB}} c_{RHB} + \epsilon_{660_{HbO_2}} c_{HbO_2} + \epsilon_{660_{COHb}} c_{COHb} + \epsilon_{660_{MetHb}} c_{MetHb}}{\epsilon_{840_{RHB}} c_{RHB} + \epsilon_{840_{HbO_2}} c_{HbO_2} + \epsilon_{840_{COHb}} c_{COHb} + \epsilon_{840_{MetHb}} c_{MetHb}} \\ \frac{A_{740}}{A_{940}} &= \frac{\epsilon_{740_{RHB}} c_{RHB} + \epsilon_{740_{HbO_2}} c_{HbO_2} + \epsilon_{740_{COHb}} c_{COHb} + \epsilon_{740_{MetHb}} c_{MetHb}}{\epsilon_{940_{RHB}} c_{RHB} + \epsilon_{940_{HbO_2}} c_{HbO_2} + \epsilon_{940_{COHb}} c_{COHb} + \epsilon_{940_{MetHb}} c_{MetHb}} \end{aligned}$$

These three equations can easily be transformed into the following linear equations in four variables:

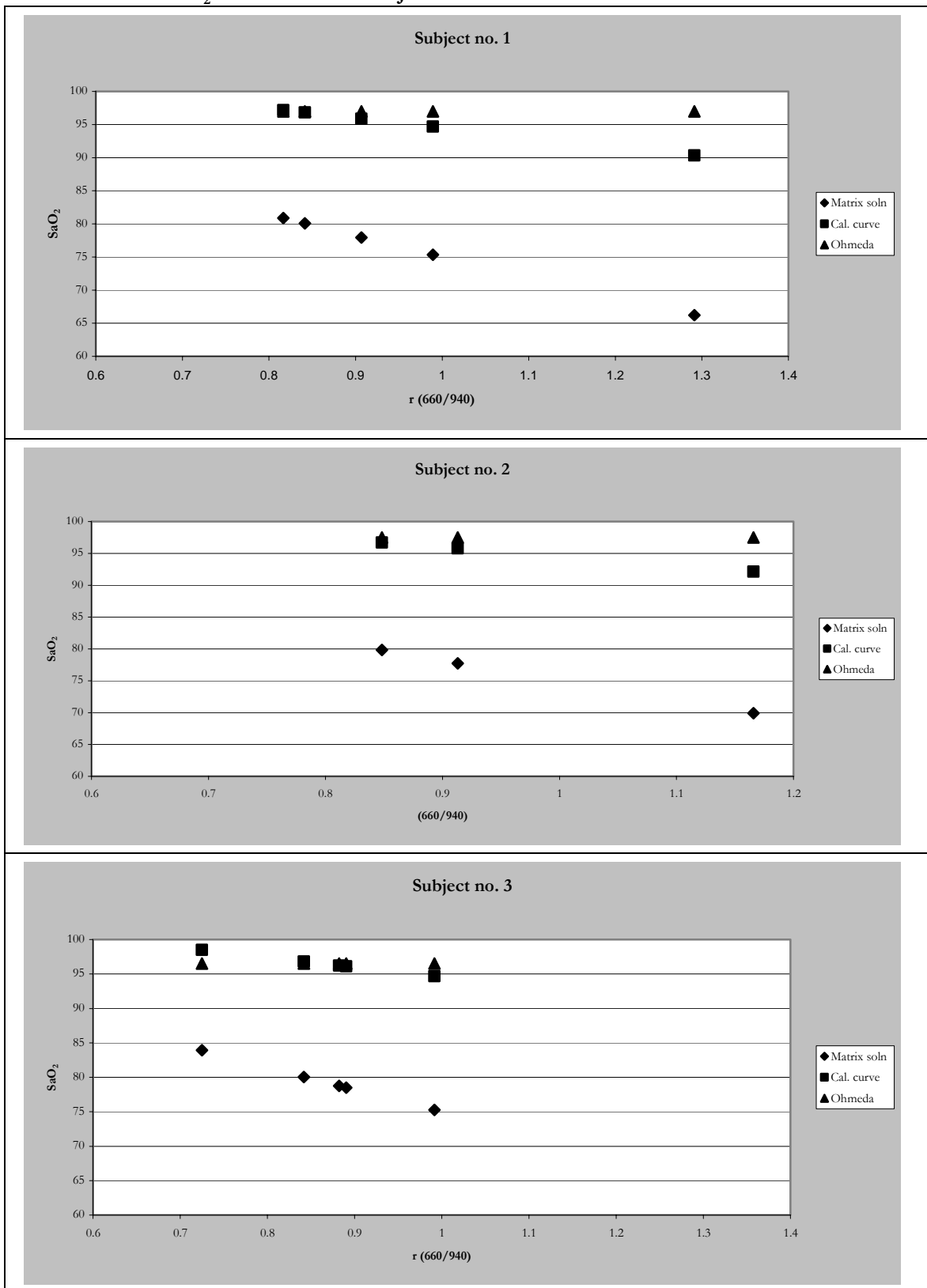
$$\begin{aligned} (A_{940} \epsilon_{660_{RHB}} - A_{660} \epsilon_{940_{RHB}}) c_{RHB} + (A_{940} \epsilon_{660_{HbO_2}} - A_{660} \epsilon_{940_{HbO_2}}) c_{HbO_2} + (A_{940} \epsilon_{660_{COHb}} - A_{660} \epsilon_{940_{COHb}}) c_{COHb} + (A_{940} \epsilon_{660_{MetHb}} - A_{660} \epsilon_{940_{MetHb}}) c_{MetHb} &= 0 \\ (A_{660} \epsilon_{840_{RHB}} - A_{840} \epsilon_{660_{RHB}}) c_{RHB} + (A_{660} \epsilon_{840_{HbO_2}} - A_{840} \epsilon_{660_{HbO_2}}) c_{HbO_2} + (A_{660} \epsilon_{840_{COHb}} - A_{840} \epsilon_{660_{COHb}}) c_{COHb} + (A_{660} \epsilon_{840_{MetHb}} - A_{840} \epsilon_{660_{MetHb}}) c_{MetHb} &= 0 \\ (A_{740} \epsilon_{940_{RHB}} - A_{940} \epsilon_{740_{RHB}}) c_{RHB} + (A_{740} \epsilon_{940_{HbO_2}} - A_{940} \epsilon_{740_{HbO_2}}) c_{HbO_2} + (A_{740} \epsilon_{940_{COHb}} - A_{940} \epsilon_{740_{COHb}}) c_{COHb} + (A_{740} \epsilon_{940_{MetHb}} - A_{940} \epsilon_{740_{MetHb}}) c_{MetHb} &= 0 \end{aligned}$$

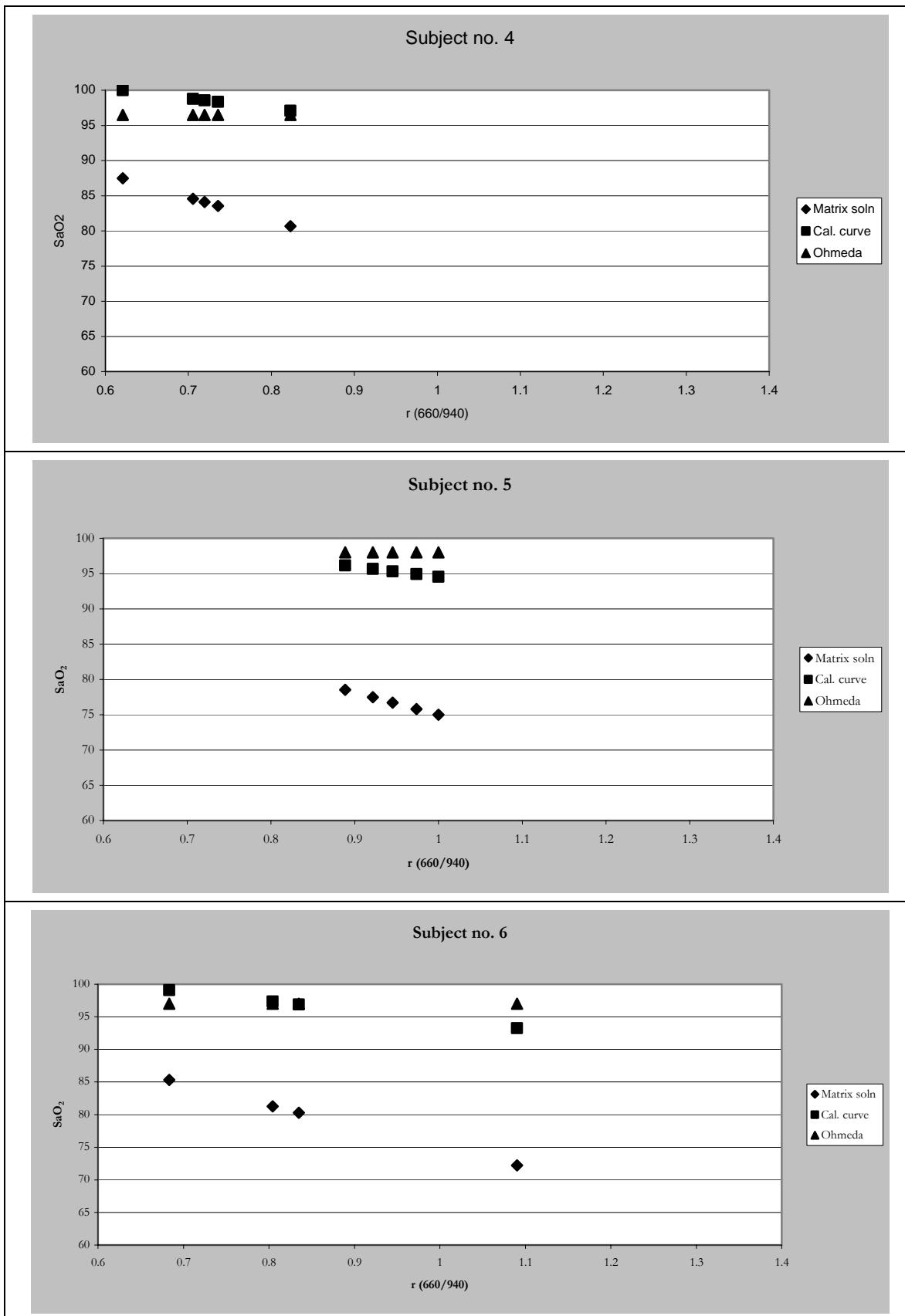
Implicit in all these equations is the assumption that only these four components exist. A fourth linear equation, then, states the sum of the four unknown concentrations as percentages for the equation:

$$c_{RHb} + c_{HbO_2} + c_{COHb} + c_{MetHb} = 100\%$$

We are allowed to express concentrations in this way because extinction coefficients may be scaled to a factor to express concentrations in whatever units are desirable, and the use of the ratio would cancel out whatever multiplicative value is necessary to convert the concentrations into percentage values. Thus, extinction coefficients may be read of any standard table with consistent units. These four equations can therefore be expressed in matrix form and solved for the four unknown concentrations as percentage values. For notational simplification, I will use the variable  $M$  to denote the coefficient that appear in the three ratio equations above

$$\begin{bmatrix} M_{r1RHb} & M_{r1HbO_2} & M_{r1COHb} & M_{r1MetHb} \\ M_{r2RHb} & M_{r2HbO_2} & M_{r2COHb} & M_{r2MetHb} \\ M_{r3RHb} & M_{r3HbO_2} & M_{r3COHb} & M_{r3MetHb} \\ 1 & 1 & 1 & 1 \end{bmatrix} \begin{bmatrix} c_{RHb} \\ c_{HbO_2} \\ c_{COHb} \\ c_{MetHb} \end{bmatrix} = \begin{bmatrix} 0 \\ 0 \\ 0 \\ 100 \end{bmatrix}$$

APPENDIX F: SAO<sub>2</sub> READINGS BY SUBJECT



## APPENDIX G: FULL TABLE OF COMBINED RESULTS

	DC (660)	DC (940)	RMS (660)	RMS (940)	r (660)	r (940)	660/940	SaO2	Cal. curve	Biox	% error
1	1.12E+03	348.8635	6.0358	2.0722	0.0054	0.0059	0.9068	77.95	95.88	97	1.154468
	1.04E+03	310.9134	3.508	1.2493	0.0034	0.004	0.8416	80.06	96.816	97	0.189374
	1.15E+03	346.0544	8.6564	2.6423	0.0076	0.0076	0.9892	75.34	94.697	97	2.374158
	1.05E+03	351.9524	5.1386	1.3321	0.0049	0.0038	1.2914	66.23	90.358	97	6.847341
	1.10E+03	381.8599	3.2753	1.3955	0.003	0.0037	0.8167	80.87	97.174	97	0.179197
2	2.58E+02	172.5582	0.9472	0.6937	0.0037	0.004	0.913	77.75	95.791	97.5	1.752671
	2.33E+02	169.7347	0.6759	0.5808	0.0029	0.0034	0.8482	79.84	96.722	97.5	0.798416
	2.21E+02	168.8767	0.8355	0.5478	0.0038	0.0032	1.1658	69.93	92.161	97.5	5.475442
3	4.15E+02	177.3514	1.0779	0.5228	0.0026	0.0029	0.8822	78.74	96.233	96.5	0.276298
	2.68E+02	171.3455	0.6781	0.5984	0.0025	0.0035	0.7249	83.92	98.492	96.5	2.06413
	2.31E+02	169.742	0.6555	0.5417	0.0028	0.0032	0.8903	78.48	96.117	96.5	0.396816
	2.12E+02	168.509	0.669	0.5373	0.0032	0.0032	0.9915	75.27	94.664	96.5	1.902546
	1.98E+02	166.6771	0.5872	0.5873	0.003	0.0035	0.8419	80.04	96.812	96.5	0.323316
4	1.49E+03	262.8536	4.9819	1.2199	0.0033	0.0046	0.7196	84.1	98.568	96.5	2.142988
	1.81E+07	477.2127	3.2465	1.3755	0.0018	0.0029	0.621	87.46	99.984	96.5	3.610033
	1.22E+03	317.0816	2.7511	1.0165	0.0023	0.0032	0.7057	84.57	98.768	96.5	2.349802
	1.66E+03	409.9134	4.4818	1.5044	0.0027	0.0037	0.7358	83.55	98.335	96.5	1.901952
	1.67E+03	390.0927	8.7677	2.4943	0.0053	0.0064	0.8231	80.66	97.082	96.5	0.603036
5	2.07E+03	663.2989	9.0937	3.1648	0.0044	0.0048	0.9218	77.47	95.665	98	2.382862
	2.23E+03	668.1748	12.566	4.242	0.0056	0.0063	0.8887	78.53	96.14	98	1.897913
	2.34E+03	716.1936	14.234	4.6001	0.0061	0.0064	0.9452	76.73	95.329	98	2.725696
	2.32E+03	745.6003	10.831	3.5706	0.0047	0.0048	0.9738	75.82	94.918	98	3.144715
	2.24E+03	741.7801	10.896	3.6154	0.0049	0.0049	1.0001	75	94.541	98	3.530037
6	7.93E+02	286.2176	1.5408	0.8133	0.0019	0.0028	0.6835	85.32	99.086	97	2.150832
	8.53E+02	273.1941	6.1976	1.8211	0.0073	0.0067	1.0903	72.21	93.245	97	3.870647
	7.62E+02	262.8148	2.0851	0.8614	0.0027	0.0033	0.835	80.27	96.911	97	0.09168
	8.10E+02	267.4804	4.5875	1.8828	0.0057	0.007	0.8043	81.28	97.352	97	0.362743

**APPENDIX H: MATLAB M-FILE FOR 4-COMPONENT MATRIX SOLUTION**

```

oximetryplus.m
function[CR,CO2, CCO, CMet]=oximetryplus(timeaq)

% [a,b,c,d]=oximetryplus(e,f,g,h)
%  accepts data acquisition from USB2000 (e,f,g,h) and returns
%  concentrations of Reduced Hemoglobin [a], Oxyhemoglobin [b],
%  Carboxyhemoglobin [c], & Methomoglobin [d].  Assumes wavelengths
%  used are 660, 940, 740 and 840; extinction coefficients stored
%  in function.

% Uses 4 equations to solve for 4 unknowns:
%
% Eq.1-3: A1/A2=[(e1Hb*CHb) + (e1HbO2*CHbO2) + (e1COHb*CCOHb) +
% (e1MetHb*CMetHb)]/[(e2Hb*CHb) + (e2HbO2+CHbO2) + (e2COHb*CCOHb) +
% (e2MetHb*CMetHb)].  e values (extinction coefficients) are known and
% defined within this function; C values (concentrations) are unknowns.
% This can be transformed into a linear equation of the form:
% [(A1e2Hb-A2e1Hb)*CHb + (A1e2HbO2-A2e1HbO2)*CHbO2 +
% (A1e2COHb-A2e1COHb)*CCOHb + (A1e2MetHb-A2e1MetHb)*CMetHb]=0.  This is
% then put in matrix form, as there are 4 coefficients for each of the
four
% unknowns.  Repeat ths process for 3 pairs of A1 and A2; selection
based
% on charts in appendix of Buinevicius thesis.
%
% Eq 4: A 4th ratio can be used. Buinevicius takes advantage of the
% assumption that Hb, HbO2, COHb, and MetHb are the only constituents
and
% use 100% = CHb + CHbO2 + CCOHb + CMetHb.  (these are percentage
values)
% All C variables are assumed to be in percentages, allowable because
the
% other equations are expressed as ratios and any conversion factor
% necessary for the extinction coefficient will therefore cancel out.

% pulsatile=ppgremez(timeaq);    % Filters to isolate pulsatile
component
% absorbances=ppga(pulsatile);    % Extracts absorbance values
% A660=absorbances(1);
% A940=absorbances(2);
% A740=absorbances(3);
% A840=absorbances(4);
%   ratio660=ppgratio(pulsatile(:,1));
%   ratio940=ppgratio(pulsatile(:,2));
%   ratio740=ppgratio(pulsatile(:,3));
%   ratio840=ppgratio(pulsatile(:,4));

%%%%%%%%%%%%%%%%%%%%%%%%%%%%%%%%%%%%%%%%%%%%%%%%%%%%%%%%%%%%%%%%%%%%%%%%
%%%%%%%%%%%%%%%%%%%%%%%%%%%%%%%%%%%%%%%%%%%%%%%%%%%%%%%%%%%%%%%%%%%%%%%%
ppg660=timeaq(:,2);
ppg940=timeaq(:,3);
ppg740=timeaq(:,4);
ppg840=timeaq(:,5);

```

```

ppg660flat=ppg660;%(600:1000);
ppg940flat=ppg940;%(600:1000);
ppg740flat=ppg740;%(600:1000);
ppg840flat=ppg840;%(600:1000);

dc660=mean(ppg660flat);
dc940=mean(ppg940flat);
dc740=mean(ppg740flat);
dc840=mean(ppg840flat);

ppg660z=ppgma(ppg660flat);
ppg940z=ppgma(ppg940flat);
ppg740z=ppgma(ppg740flat);
ppg840z=ppgma(ppg840flat);

ppg660zf=ppgremez(ppg660z);
ppg940zf=ppgremez(ppg940z);
ppg740zf=ppgremez(ppg740z);
ppg840zf=ppgremez(ppg840z);

rms660=sqrt(mean(ppg660zf.*ppg660zf));
rms940=sqrt(mean(ppg940zf.*ppg940zf));
rms740=sqrt(mean(ppg740zf.*ppg740zf));
rms840=sqrt(mean(ppg840zf.*ppg840zf));

A660=rms660/dc660;
A940=rms940/dc940;
A740=rms740/dc740;
A840=rms840/dc840;

% Defines coefficients for O matrix (y=O*x)using beereqn function for
first
% three equations in 4x4 matrix

[eq1]=beereqn(A940,A660,940,660); % A940/A660
[eq2]=beereqn(A660,A840,660,840); % A660/A840
[eq3]=beereqn(A740,A940,740,940); % A740/A940
[eq4]=[1 1 1 1];

% Solves matrix equation of the form:
% [ 0] [O11 O12 O13 O14] [ CHb ]
% [ 0] = [O21 O22 O23 O24]*[ CHbO2 ]
% [ 0] [O31 O32 O33 O34] [ CCOHb ]
% [100] [O41 O42 O43 O44] [ CMetHb ]

O=[eq1;eq2;eq3;eq4];
C=inv(O)*[0;0;0;100];
CR=C(1);
CO2=C(2);
CCO=C(3);
CMet=C(4);

```

**APPENDIX I: MATLAB M-FILE FOR 2-COMPONENT MATRIX SOLUTION**

```

Oximetry3.m
function [r, saO2]=oximetry3(timeaq)

ppg660=timeaq(:,2);
ppg940=timeaq(:,3);
% ppg740=timeaq(:,4);
% ppg840=timeaq(:,5);

ppg660flat=ppg660(600:1000);
ppg940flat=ppg940(600:1000);

dc660=mean(ppg660flat)
dc940=mean(ppg940flat)
% dc740=mean(ppg740flat);
% dc840=mean(ppg840flat);

ppg660z=ppgma(ppg660flat);
ppg940z=ppgma(ppg940flat);
% ppg740z=ppg740flat-mean(ppg740flat);
% ppg840z=ppg840flat-mean(ppg840flat);
%
ppg660zf=ppgremez(ppg660z);
ppg940zf=ppgremez(ppg940z);

rms660=sqrt(mean(ppg660zf.*ppg660zf))
rms940=sqrt(mean(ppg940zf.*ppg940zf))
% rms740=sqrt(mean(ppg740z.*ppg740z));
% rms840=sqrt(mean(ppg840z.*ppg840z));

r660=rms660/dc660
r940=rms940/dc940

r=r660/r940;

%applies calibration curve
e660Hb      = .81;           %0.79;
e660HbO2    = .08;
e940Hb      = .18;           %0.2;
e940HbO2    = .29;

saO2=(e660Hb-e940Hb*r)/((e660Hb-e660HbO2)-(e940Hb-e940HbO2)*r);

```

**APPENDIX J: MATLAB M-FILE FOR BAND-PASS FILTERING**

```
ppgremez.m
function [ppgfilter]=ppgremez(waveinput)
% [a]=ppgremez(waveinput)  Calculates 101-pt optimized
%                          filter window and returns
%                          filtered wave inputs (4 wavelengths)
%                          Returns 0s if no 3rd and 4th wavelength

%% Derives 101-pt optimal filter
d=0.01;
F=[0 0.051-d 0.051+d 0.4-d 0.4+d 1];
A=[0 0 1 1 0 0];
b=firpm(101,F,A);
ppgf=filter(b,1,waveinput);
[m,n]=size(ppgf);
ppgfilter=ppgf(102:n);
```